ARTICLE

Toward Intelligent Synthetic Neural Circuits: Directing and Accelerating Neuron Cell Growth by Self-Rolled-Up Silicon Nitride Microtube Array

Paul Froeter,[†,▽] Yu Huang,[⊥,#,▽] Olivia V. Cangellaris,[‡] Wen Huang,[†] Erik W. Dent,[¶] Martha U. Gillette,[‡,§] Justin C. Williams,[*,⊥] and Xiuling Li[*,†]

[†]Department of Electrical and Computer Engineering, Micro and Nanotechnology Laboratory, [‡]Department of Bioengineering, and [§]Department of Cell and Developmental Biology, University of Illinois at Urbana—Champaign, Urbana, Illinois 61801, United States, [⊥]Department of Biomedical Engineering, University of Wisconsin-Madison, Madison, Wisconsin 53706, United States, and [¶]Department of Neuroscience, University of Wisconsin-Madison, Madison, Wisconsin 53705, United States. [▽]These authors contributed equally to this work. [#]Present address: Department of Nanomedicine and Biomedical Engineering, Houston Methodist Hospital Research Institute, Texas Medical Center, Houston, Texas 77030.

ABSTRACT In neural interface platforms, cultures are often carried out on a flat, open, rigid, and opaque substrate, posing challenges to reflecting the native microenvironment of the brain and precise engagement with neurons. Here we present a neuron cell culturing platform that consists of arrays of ordered microtubes (2.7−4.4 μm in diameter), formed by strain-induced self-rolled-up nanomembrane (s-RUM) technology using ultrathin (<40 nm) silicon nitride (SiN_x) film on transparent substrates. These microtubes demonstrated robust physical confinement and unprecedented guidance effect toward outgrowth of primary cortical neurons, with a coaxially confined configuration resembling that of myelin sheaths. The dynamic neural growth inside the microtube, evaluated with continuous live-cell imaging, showed a marked increase (20×) of the growth rate inside the microtube compared to regions outside the microtubes. We attribute the dramatic accelerating effect and precise guiding of the microtube array to three-dimensional (3D) adhesion and electrostatic interaction with the SiN_x microtubes, respectively. This work has clear implications toward building intelligent synthetic neural circuits by arranging the size, site, and patterns of the microtube array, for potential treatment of neurological disorders.

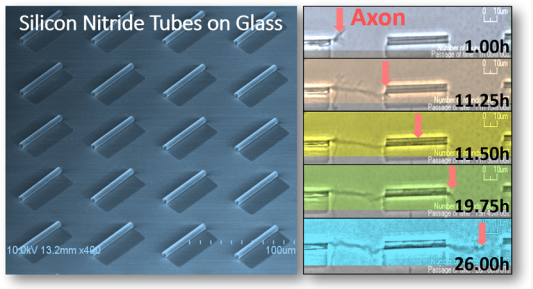

KEYWORDS: neural culture · neural-electrode interface · silicon nitride nanomembrane · axon guidance · pathfinding

There is a growing demand for reliable neural-electrode interfaces, as their development has continuously made crucial impacts in the field of neuroengineering, including the understanding of brain cognition, implementation of neuroprosthetics, and treatment of neural degenerative diseases.[1−3] Tremendous efforts have been divergently directed to build complex neural culturing platforms[1,4−6] and efficient electronic devices.[7−14] However, an optimal integration of these two systems on the same substrate/interface is far from reality, posing serious challenges to support the next-generation neural interface.

A major disadvantage of the commonly used substrate materials for neuron culture, such as bulk metal and inorganic semiconductor, is their low biocompliance and poor optical properties. On one hand, a native brain environment is extremely soft with an elastic modulus in the range of 0.1−10 kPa,[15] while the substrates are significantly stiffer with an elastic modulus on the order of 10−200 GPa. Such a vast discrepancy introduces a mechanically distorted microenvironment to surrounding neurons, influencing cell behavior (development, outgrowth, migration, *etc.*) and misrepresenting neural network function.[16−18] At the tissue level, low biocompliance may further abolish the *in vivo* use of an electrode interface, by inducing electrode-tissue micromovement and subsequent immunological rejection.[19,20]

* Address correspondence to xiuling@illinois.edu, jwilliams@engr.wisc.edu.

Received for review August 29, 2014 and accepted October 20, 2014.

Published online October 20, 2014
10.1021/nn504876y

On the other hand, high opacity and low optical clarity of existing substrate materials hinder the integration of neuro-photonic technology and modern microscopy.[7] Such integration is highly desirable because these emerging technologies provide revolutionary tools for neural stimulation (i.e., optogenetics[21]) and monitoring (e.g., cranial window imaging,[22]), with minimal invasiveness, high accuracy, and high-resolution.

Another challenge comes from the lack of confined guidance and intimate contact to small diameter axons. This often leads to low signal-to-noise ratio (SNR) and poor fidelity over time, especially when high-resolution recording (e.g., single neuron level) is desired. The measured action potential of individual neurons is often diminutive (on the order of microvolts), decaying rapidly over distance, and easily lost among background noise.[23−27] Therefore, measurable electronic coupling between electrode probes and neuronal membranes requires a close vicinity or even direct contact, which often relies on neural guidance through printed adhesives.[5,28−30] However, the adhesive guidance does not guarantee a nifty contact and is often subject to subsequent protolytic degradation. Neurons may translocate and migrate out of electrode detection range. Furthermore, within brain tissue, implantation and other coculture systems, supporting cells (*e.g.*, glia) may cause problems by migrating into electrode-neuron interspaces and forming low-conductive barriers.[19,20] To avoid these issues, an ideal interface should provide confined guidance that allows for contact with the electrodes in an enclosed space and exclusion of nearby cells, maximizing the signal quality. Here, we demonstrate a novel approach, strain-induced self-rolled-up silicon nitride (SiN_x) microtubes on a transparent substrate, which overcomes the above-described challenges and presents an ideal substrate for next-generation neural interface.

Strain-induced self-rolled-up membrane (s-RUM) technology, in which 2D membranes self-assemble into 3D tubular architectures at the micro- and nanoscale driven by built-in strain, is well positioned for extreme miniaturization and integration of photonic, electronic, mechanical components, and biomedical applications.[31−36] Ultrathin membranes possess novel qualities that are particularly attractive to tissue engineering, such as the improved optical transparency and mechanical properties that match to cell stiffness.[37,38] S-RUMs have recently been shown as a promising platform to investigate cell outgrowth during culture.[39−41] Unlike polymer channels that confine growth in one and a half dimensions, microtube-based substrates provide complete radial confinement as well as an opportunity to create complex material combinations.[32,39−41] Optically transparent materials can also achieve self-rolled-up tubular structures, advancing the study of general cell guidance and electro-photonic interaction. One previous example consisted of multilayered $SiO_x/SiO_2/Al_2O_3$ microtubes.[39] The mouse motor neurons used in said study exhibit enthusiastic interaction with the microtubes. However, at the diameter of 15 μm, these microtubes were far beyond the dimension required to confine axons. It was also reported that axons exhibit a general tendency to grow through semiconductor microtubes that consisted of dual-layered NMs (SiGe/Si, GaAs/InGaAs).[40,41] In this case, the range in diameter was proper for single axon guidance, but, since the carrying substrate materials are opaque, cell growth dynamics were difficult to monitor through live-cell imaging.[40,41] The initial success in achieving some degree of axon guidance left many important questions regarding the cell-material dynamic interaction that remained to be answered.

Our recent progress on the s-RUM technology made it possible to engineer microtubes with SiN_x NMs on a broad range of substrates, offering further advantages to address these pivotal questions.[42,43] Rolling-up a SiN_x NM involves a highly simplified fabrication process that uses a dual-frequency deposition in the same plasma-enhanced chemical vapor deposition (PECVD) tool to engineer the strain. Unlike those approaches using bi/multilayer epitaxial growth that were restricted to a lattice mismatch range, our method works with virtually any substrates and any biocompatible sacrificial layers. This offers unprecedented flexibility in the selection of substrates for various functions. For example, one can make microtubes on bendable substrates for flexible integration, on soft polymers for biomechanical study, and on transparent glass slides for optical characterization and manipulation. Furthermore, PECVD makes it possible to independently tune material properties and composition, affecting porosity, capacitance, index of refraction, and hydrophobicity. In this study, we demonstrate a neuron cell culturing platform using SiN_x s-RUMs on a German glass coverslip, a widely used neural culture substrate for its excellent surface smoothness and optical quality. Primary cortical neurons were cultured on the platform to study axon guidance and cell-material interaction. After plating with primary neural culture, the SiN_x microtubes (diameter ~2.7−4 μm) provided spatial guidance for the growing axons. It was through the long-term time-lapse live-cell imaging that we found cells actively explore the substrate for a tubular opening. Once the growth cone entered a tube, the axon extension was accelerated up to 20 times its normal growth rate.

RESULTS

Robust Guiding and Delineating Effect. To provide 3D scaffolds that guide and confine individual axons, the size of the microtube needs to be precisely controlled at a slightly larger diameter than that of a typical axon (2−3 μm). Smaller microtubes failed to sustain

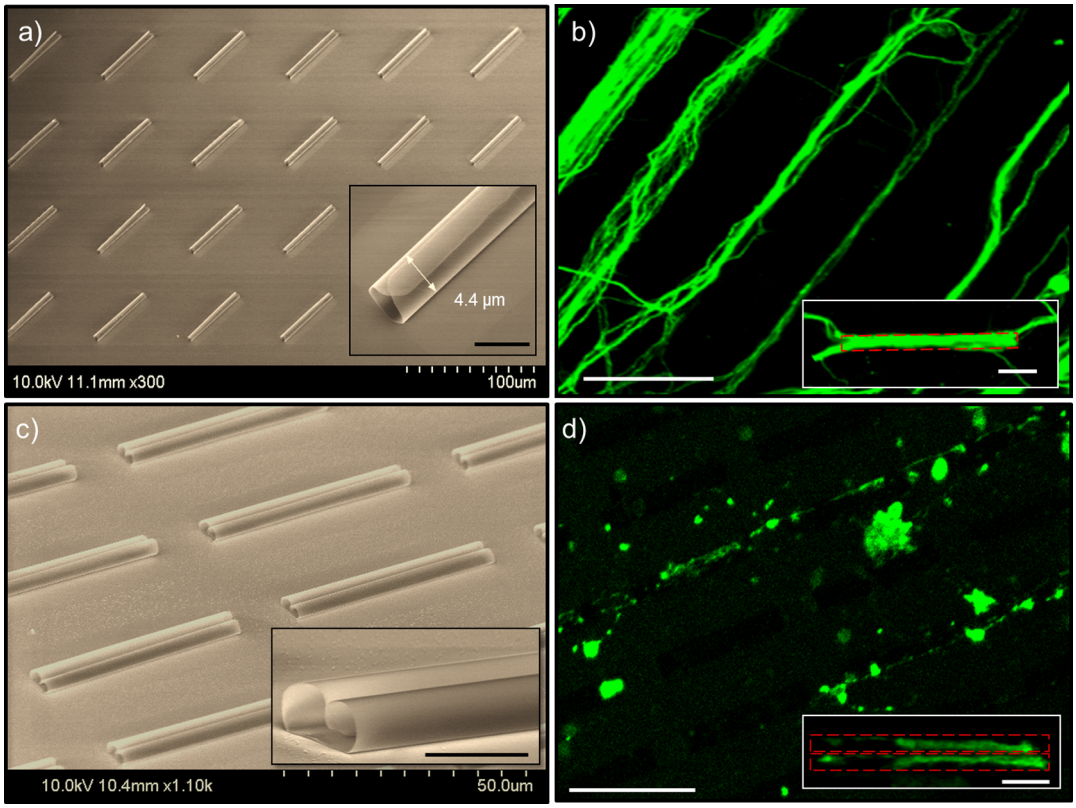

Figure 1. SEM images (a and c) of SiNx microtube array and the corresponding immunocytochemistry of neural culture fluorescence images (b and d). (a) Single roll and (c) binocular-shaped double roll SiNx microtube array on a Si (111) substrate. Close-up SEM images show fully enclosed 3D tubular scaffolds, with diameters of 4.4 μm (1a inset) and 2.7 μm (1c inset), and length of 50 μm. The scale bars in insets represent 5 μm. (b) High- and (d) low-density seeded neuron culture, fluorescently labeled for axon localization, using the microtube arrays in panels a and c, respectively, showing a strong tendency to continuously follow the microtube array in a linear trajectory (scale bar: 50 μm). Individual axons are confined and delineated by the microtubes (b and d insets, scale bars, 10 μm).

inner-tubular growth, while tubes that are too large tend to include multiple axons or even neural soma.[40] For the SiN_x microtubes used in this study, a proper diameter was achieved by controlling the thickness of the tensile and compressive stressed layers in the deposition process. Fabrication details were reported previously[42] and summarized in the Methods section of this study.

To demonstrate the general guidance effect of tubular structures, a large array of SiN_x microtubes was employed. Figure 1a shows a 4 $\times$ 6 array of such tubes on a silicon substrate, that are 4.4 μm in diameter (Figure 1a inset) and 50 μm in length. The pitch is 40 μm in the longitudinal direction and 50 μm in the transverse direction. A cortical neuron cell culture was seeded on this substrate. As shown by immunocytochemistry (Figure 1b) of fluorescently labeled tubulin, the resulting neuron outgrowth forms bundles, similar to those guided by adhesion pattern and microfluidic channels.[5,44,45] The axon bundles robustly follow the microtube geometry and array layout with a preferential linear path along the axial direction of the microtubes. For most of the bundles, guidance was observed along both the inside (Figure 1b inset) and outside of the microtubes (e.g., the bundle in the upper left of Figure 1b is obviously wider than the microtube diameter). To identify whether the piloting axon was guided inside or outside, we seeded low-density cultures on an array of binocular-shaped SiN_x microtubes, so the neurons were sparse enough to avoid forming bundles. The binocular tubes are formed when the rolling takes place simultaneously on both sides for NMs (with width equal to two circumferences) to form double rolls. Shown in Figure 1c, the binocular samples have two side by side microtubes of 2.7 μm diameter, 20 μm longitudinal spacing, and 50 μm transverse spacing. This structure sufficiently guides single axon extensions, with each confined inside one of the double channels and clearly delineated, as seen in Figure 1d. The resulting immunocytochemistry of the cells shows extending single axons that colocalize strictly within the binocular microtube pattern in pairs (Figure 1d inset) in most cases, suggesting the initial guidance was most likely through the inside of the microtube. In the case of high seeding density, microtubes that are plugged by a neuron or occupied by an axon of comparable diameter (Figure 1b) result in successive processes guiding along the outside of the microtube. Using binocular shaped microtubes, the tube walls not only effectively separate parallel

processes (Figure 1d inset), but also provide a better scaffold for separating extensions as the culture matures. This is further supported by 3D rendering of the confocal images, available in the Supporting Information, Figure S5. Because of these attributes, binocular microtube architecture is attractive when designing an interface that couples discretely with parallel processes bundled in complex networks.

Supporting Information, Figure S5 also reveals that the axons grown through the tubes take on different morphology as compared to those outside of tubes. By comparing the height difference between the neurons grown along the outer edge (e.g., Neuron A) and inside (e.g., Neuron B) the binocular microtube structures, we can see that the axons grown inside appear to take on the shape of the microtubes by filling the tube inner space for the most part with a height of ~2 μm. In contrast, the axons grown outside the tube tend to flatten out showing a height no more than 1 μm.

Remarkably, the axons persistently maintained the same path in the open planar area between the microtubes for all the spacing (20−40 μm) we examined. At 20 μm spacing (Figure 1c), the axons followed successive collinear tubes with very little divergence from the binocular microtube array. By increasing the spacing to 40 μm (Figure 1a), a larger and more complex network emerges, but still maintains an overall linear order (Figure 1b). Based on all the fluorescent images examined (Figure S6), the fraction of axons that follows the linear path is estimated to be ~83%. This faithful linear guidance is in sharp contrast to other guidance platforms reported (printed adhesion, microfluidic channels, *etc.*) where axons immediately branch out in nonconfined regions.[45] It is of great interest for neural physiological study to provide nonconfined regions without disrupting guidance. For instance, such regions can be pin-pointed for access of chemical perfusion and patch-clamp. Furthermore, similar to the internodal segment of myelin, these unbound regions allow ion exchange with a culture medium at selected regions.[46] This may serve as the structure basis for salutatory conduction that further facilitates signal transduction efficiency of neurons in the application of neural interfaces.[47−49] We can infer linear guidance from fluorescent imaging, with localized static and two-dimensional cell positions, but not necessarily whether the processes grow within the microtube or along the outer wall, given the ultrathin NM. To further understand how neurons respond to the microtube's 3D geometry, especially in a dynamic aspect, live-cell imaging and SEM is desired.

Acceleration in Growth Rate. Neural guidance and cell-material interaction are highly dynamic processes, the capture of which would provide key information toward understanding the underlying mechanism. Information from static images such as those described above is often inferred and sometimes misleading. To investigate dynamic interactions between neurons and microtube substrates, live-cell imaging was performed on a cortical neural culture (E15.5), by monitoring cell morphological change over a period of 12−36 h. Such an approach requires a fully transparent platform. Opaque substrates such as Si would be incompatible. Taking advantage of our method, we fabricated SiN_x microtubes directly on German glass coverslip, an optimal transparent substrate that is commonly used for neural imaging. A silicon dioxide-coated glass coverslip also provides greater fluorescent resolution and enables the collection of confocal z-stacks and three-dimensional rendering. A SiN_x microtube array, with desired size and pitch, monolithically fabricated on glass slides serves as the perfect high quality, fully transparent scaffold for live-cell imaging.

Figure 2a shows a typical axonal outgrowth on a SiN_x microtube array in five frames from live-cell recording (Supporting Information, video S1a) of 33.75 h. As visualized in these frames, cell movement such as growth cone outgrowth on such a transparent substrate can be accurately traced in phase contrast, while avoiding photodamage to neurons that often accompanies fluorescent imaging. At time 0:00, the axonal growth cone explored the path of outgrowth on the planar glass substrate. At time 11:15 and 12:30, the growth cone contacted the inlet and extended into the microtube, respectively. At time 19:45 and 26:45, it exited out of the microtube and grew back onto the planar substrate, respectively. Axonal outgrowth and pathfinding are primarily governed by dynamic microtubule/F-actin interactions and corresponding filopodia dynamics in response to sensed substrate cues.[50] Visible in Figure 2a and the original time lapse of video S1a, between frames 11:15 and 12:30, dynamic retraction and simultaneous extension of filopodium were often observed at a certain distance range (~20 μm) in the direction of the microtube. This suggests existence of sensory processes with length in that range to be identified in a future study. In video S1a it is evident that neural growth cones exhibit a strong and active pathfinding capability toward the microtube opening.

Live-cell imaging was used to compare the outgrowth speed of the axon inside and outside the microtube, showing a drastic acceleration as the growth cone enters the microtube (Figure 2b). As seen in Figure 2b, the axon outgrew onto and traversed 40 μm of the flat coverslip between microtubes at a rate of ~2−7 μm/h. As the growth cone grew into the microtube, that speed increased by ~20 fold in the first half of the microtube. Although the process slowed down as it navigated the microtube, the speed within the microtube was still much higher (~4×) than that on the planar substrate. After the growth cone exited the microtube, it extended back onto the planar

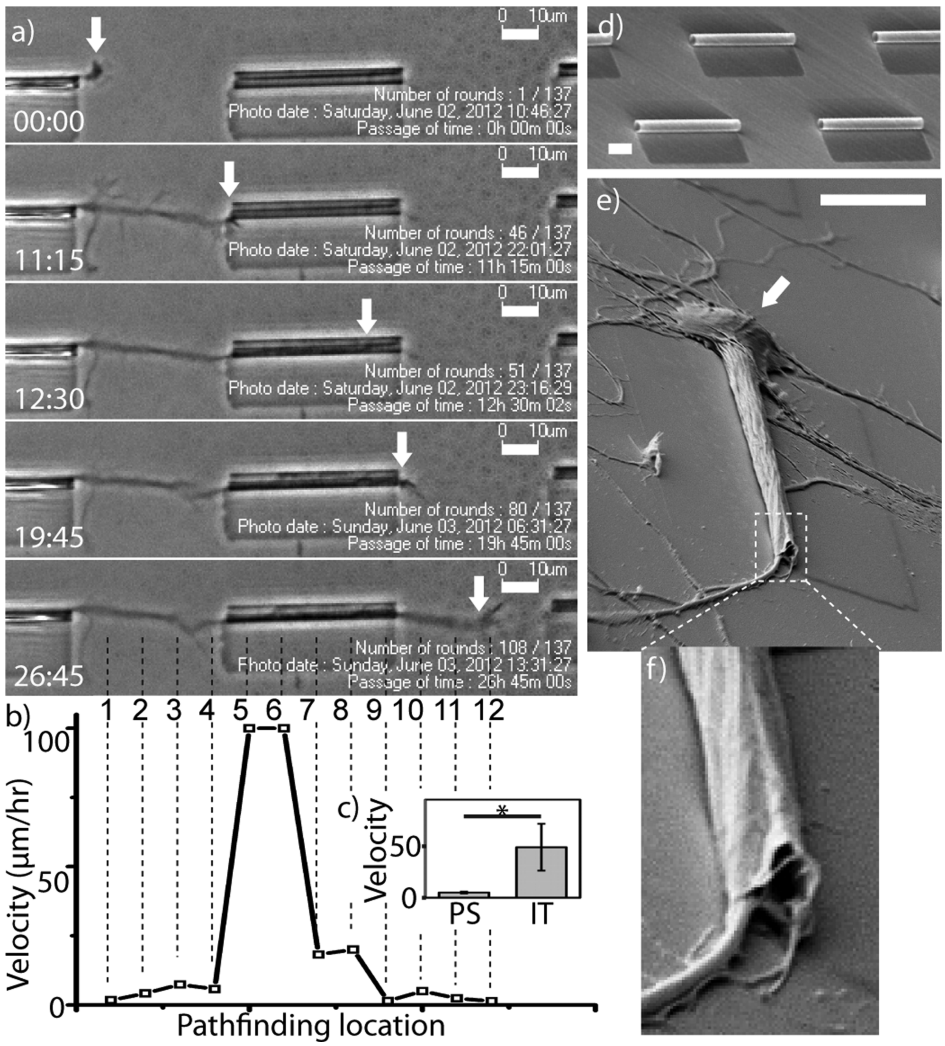

Figure 2. Outgrowth of a single neuron in a microtube. (a) Time-lapse phase contrast images of a living cortical neuron show axonal pathfinding through a microtube. Each frame, from top to bottom, represents growth cone's location (arrows) at key time-points (from top to bottom): 0:00, on planar glass substrate; 11:15, at tube inlet; 12:30, inside tube; 19:45, at tube outlet; 26:45, back on planar glass substrate. Time is denoted in hh:mm. Original videos of live recording are included in Supporting Information. (b) Outgrowth velocity chart shows a ~20× acceleration as the axon extended into tubes (location #4 → #5), and decelerated to its original level while exiting onto planar substrate (location #8 → #9). Velocity was calculated for each pathfinding locations at 10 μm interval, on the basis of a live-cell recording. Each of 12 locations is marked by a numbered vertical broken-line in the last time lapse image (26:45). (c) Outgrowth velocity (μm/h) inside tube (IT) is significantly higher (12× on average) than that on planar substrate (PS) on a level of $p = 0.05$. (d) SEM image of the culturing substrate that contains an array of microtubes on transparent glass substrate. The fabrication detail is described in the Methods section. (e) SEM image of a single matured neuron growing in a microtube shows SiN_x NM topographically conforms to the cellular surface and excludes the cell body (arrow). (f), Confirmation of microtube deformation at exiting end (~2 μm minimum dimension), forming an enclosure and tight cell contact. (Scale bar, 10 μm).

substrate and the outgrowth speed dropped back to <7 μm/h. Similar enhancement was observed in other instances of confined guidance (e.g., microfluidic channels), however, less drastic (2−3 fold) according to our unpublished observation and others' publications.[51,52] We speculate that the greater speed also correlates with the limited branching nature of the axon in such confined spaces. According to the actin treadmilling model,[53] the overall actin polymerization (extension or branching) is conserved. So when the branch is limited by spatial confinement, actin polymerization is likely to be more distributed for extension. The more confined the axon is, the more biased this distribution is likely to be, therefore, speeding up axon outgrowth.

It is worth noting in frame 11:15 of Figure 2a that the axon deflects ~1 μm from its path. This same attraction is seen uniformly across samples, and appears to have an effective radius of 5 μm. This minor deviation seems to result from the facilitated pathfinding effect by the substrate-bound NM sheet that forms a ~100 nm tall ridge (Figure 2e). During *in vitro* cultures, neural growth cones maintain close contact with the substrate and are therefore sensitive to such topographic cues. Sending processes along the ridge, the growth cone may eventually migrate to the more attractive tubular

scaffold. A similar effect is observed with cortical neurons that attach near the long side of the microtube and send processes out toward the microtube sidewall, only to be restricted by the small gap between the microtube and substrate, successively retracting toward a less restrictive area. If the neuron is close enough to the opening of another microtube, however, the process will retract and divert into the open microtube (Supporting Information video 1).

DISCUSSION

Several characteristics of the SiN_x microtubes may contribute to the enhanced axon guidance and growth within the microtubes. One major factor is the 3D tubular scaffold that provides complete radial confinement to axons. It was widely observed that neurons tend to extend processes into confined spaces, including grooves,[5] channels,[44] tubes,[40] and even micromazes. These spaces are commonly believed to provide enclosed 3D topography to enhance cytoskeletal tension of the growth cone, desirable for axon extension or branching. Under this hypothesis, the tubular structure should provide optimal guidance to the axon since cytoskeletal tension is maximal with a coaxially wrapped configuration, similar to the native topographic environment (e.g., myelin) of the neuron.

Another influencing factor could be the mechanical compatibility and compliance of the ultrathin walled microtubes to the environment of neuron growth. It is known that although bulk PECVD SiN_x film has a relatively high Young's modulus,[54] as the film thickness falls in the nanometer range, the bending modulus becomes much smaller.[55] This is beneficial, since neurons exhibit increased outgrowth on substrates with a lower stiffness.[56] Furthermore, as shown in Figure 2e,f, with a wall thickness of only 40 nm, we have observed that the tubular membrane became conformal to the axon topography when the cell matured (2 weeks (14 DIV)), and the axon's diameter increased to a comparable size as the microtube. Figure 2e reveals a typical polarized neural morphology with a putative single axon confined through the microtube, extended 50 μm with its soma excluded at the tube opening. Unlike the previously reported tube-cell contact (with tube diameter of >5 μm),[40] our microtube is significantly smaller (tube diameter of $\sim$2−4 μm). As a result, the axon exhibits much tighter contact with the NM as shown in Figure 2e, especially at the microtube opening toward the cell soma. In addition, the SiN_x microtube also demonstrated high biocompliance toward the axon, as its wall membrane tightly conformed to the cell membrane around the axon (Figure 2e, f). In addition, the axon hillock is fully seated in the microtube while the NM tightly conformed into a tapered geometry, which further enhances NM−cell contact. This is different from cell-free s-RUM samples (Figure 2d), where microtubes maintain smooth surfaces and a consistent diameter over the entire length. Clearly, tight contact offers advantages to support a neural interface by enhancing signal/noise ratio at recording, excluding undesired cell species, and isolating the ionic environment. Herein displayed biocompliance made such advantages even more practical. For instance, with the microtube architectures that expand and contract in compliance with the axon, a uniform array of microtubes can flexibly fit cells of various diameters. Furthermore, this unique property makes it possible to support a long-term neural interface that accommodates the increasing diameter of a maturing axon.

There is no doubt that geometrical confinement due to the 3D structure and compatible stiffness are important contributing factors in the superior guidance and growth enhancement effect of SiN_x microtubes observed. On the other hand, it is also known that electrostatic interaction between the cells and substrates plays a crucial role in biocompatibility, by influencing protein adsorption,[57,58] cell adhesion,[59] proliferation,[58] and survival.[60] Many commonly used culture substrate materials (*e.g.*, silica, alumina, titania) have a negative zeta potential (negatively charged on surface) at physiological pH, requiring PDL coating to achieve a positive charge and enhanced adhesion. In contrast, SiN_x, with a positive zeta potential can promote cell contact during seeding and maintain it thereafter.[61] The charge/electric-field distribution may further enhance axon extension toward the interior of the microtube. Fortunately, at physiological pH, the surface charge of the SiN_x bilayer is mild enough to avoid undesired protein coagulation and adsorption. When considering biodegradability, the Hamaker constant will be the dominant property, as it can be used to determine the critical coagulation concentrations as a solution's iconicity increases.[62] The SiN_x presented in this study, with a Hamaker constant of 1.9×10^{-20} J, is significantly better at avoiding coagulation when compared to alumina, 4.1×10^{-20} J, and well within the range of approved biocolloids, 3×10^{-21} to 4×10^{-20} J.[62]

To quantify the trapped charge density in the SiN_x bilayer film, metal/insulator/semiconductor (MIS) capacitors were fabricated on n-type silicon wafers with the I layer being 200 nm of high frequency (HF) SiN_x (inner tube wall) or 200 nm of low frequency (LF) SiN_x film (outer tube wall). Although the films used in these capacitors were thicker than the bilayer used in the rolled-up microtubes, identical deposition conditions were used. The SiN_x samples were capped with aluminum and subjected to capacitance−voltage measurements, sweeping over large negative and positive ranges to observe trapped charge dependent flat band voltage shifts (Figure 3a). We observed flat band voltage shifts of −25 and −18.5 V for the 200 nm thick HF and LF SiN_x films, respectively. The extracted fixed charge density would therefore be 4×10^{11} cm^{-2} in the 20 nm HF-SiN_x and 3.3×10^{11} cm^{-2} in the 20 nm

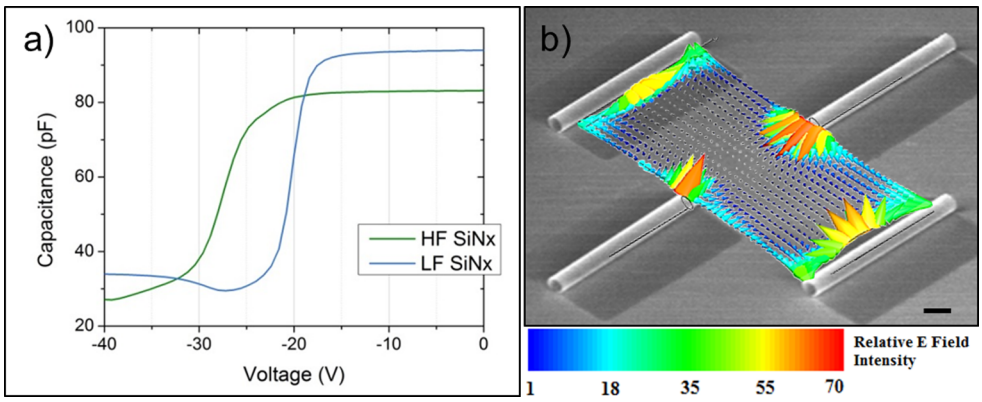

Figure 3. Electrostatic effect of SiN_x microtubes. (a) High frequency capacitance−voltage (*C*−*V*) measurement of tensile HF- and compressive LF-SiN_x reveals a large flat band voltage shift to the left, indicating a large quantity of fixed positive charges within the film. (b) Superimposed SEM (in grayscale) of microtube array (10 μm scale bar) with respective mapping (in color) of electric field vectors between 40 μm pitch microtube arrays. Relative *E* field intensity is obtained from quasi-static FEM simulation when the side wall charge density is 36% of that at the tube opening (values are normalized to the minimum *E* field intensity). For more information about the FEM simulation see the Supporting Information.

LF-SiN_x, assuming fixed charges are uniformly distributed.[63] The details on the extraction process are provided in the Supporting Information.

The extracted charge density values were then used to map out the electric field lines of microtube arrays of different layouts. To find the static electric field distribution in areas between microtubes, a quasi-static FEM simulation performed using the High Frequency Structure Simulator (HFSS v.11) based on the charge density extracted from the C−V analysis. Details of the simulation method can be found in the Supporting Information. Figure 3b presents a simulated electric field line spatial map emanating from the trapped positive charges in the SiN_x microtubes with the same layout as in Figure 2d. It can be seen that the field intensity is greatest near the opening of the microtube, but radiates from both microtube openings and sidewalls. This is sensible as both films comprising the microtube walls are positively charged, with greater charge density trapped in the HF film that lines the inside of the microtube. The electrostatic analysis suggests that trapped positive charges in the SiN_x microtubes can also be responsible for the persistent guiding and enhanced growth of axons. Naturally, the electric field intensity between microtubes increases as pitch decreases, consistent with the enhanced linearity observed with closer spacing between tubes as shown in Figure 1b,d.

CONCLUSION

In summary, we have demonstrated that self-rolled-up SiN_x microtube arrays provide extremely well-defined guidance and dramatically increased growth rate for cortical neuron cells. These microtubes are easy to fabricate, versatile in morphological and electrostatic properties, and precisely controllable in geometry, all by conventional planar processing before rolling-up. The biocompliant and biocompatible nature, along with the universal applicability to any substrates, also makes these microtubes ideal for integration. In a typical neural environment, neurons grow quite slowly and mostly connect in their immediate vicinity. The ability of the microtube array to control the speed and direction of axonal extension provides a key element in arranging patterned neural networks that have both short and long-range connections. By patterning the microtubes with desired diameter, orientation, length, and spacing, as well as hierarchical tubular network with in-plane and out of plane geometry variations,[65,66] complex and intelligent synthetic neural circuits are within reach. Furthermore, the coaxially confined and periodically spaced axon-in-a-tube configuration resembles that of myelin sheaths and Ranvier node in the nervous system. Future directions will include roll-up other functional structures such as multiple electrode arrays (MEA) with the SiN_x microtubes, to provide an ideal route for integration of electrodes into neural cultures. Coupled with photonics, this rolled-up micro-MEA can directly monitor the dynamic neural activities and record action potentials with better resolution and accuracy than the state-of-art cuff electrodes. With continued research at the single cell as well as at the network level, we are confident that this innovative neuro-nanotechnology platform will stimulate new research directions and bring new discoveries in the field of neural regeneration.

METHODS

SiNx Bilayer Deposition, Microtube Fabrication, and Morphology/Topology Tuning. For the thin membrane to roll, sufficient strain must be embedded in the film, placing a constraint on the system. Compressive strain must be embedded in at least a fraction of one component to provide an expanding force, followed by one of two actions. The method used in this study relies primarily on changing the plasma frequency.[42] Alternatively, one can begin

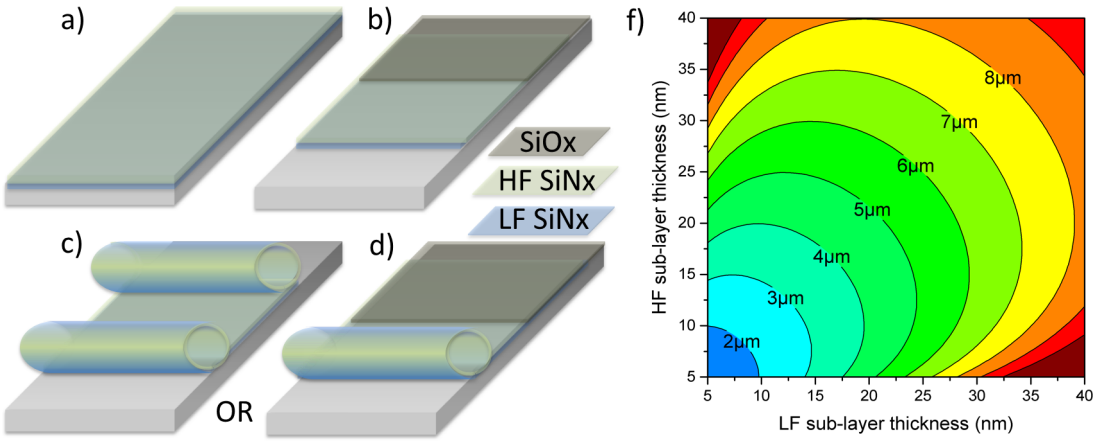

Figure 4. Fabrication process for a rolled up SiNx microtube: (a) deposition of sacrificial layer and compressively strained LF layer, followed by deposition of tensile strained HF-layer; (b) formation of rectangular mesa (optional) deposition of 100 nm PECVD SiO_x anchor, and either released from (c) both sides (process #1) or (d) one side (process #2). In both processes, the initial pad dimensions determine the final geometry. (f) Microtube diameter is determined by both LF and HF layer thickness. The deriving mathematics was previously described.[42]

the plasma deposition at a higher temperature, reducing temperature as deposition proceeds.[32] As seen in Figures 1 and 2, two methods are employed to achieve microtube arrays (Figure 4), depending on etchant speed and uniformity: timed etching (process #1) and anchored membranes (process #2), for slow and fast etches, respectively. This study focuses on the former to achieve single and binocular shaped microtubes on silicon substrates. The latter is employed during live-cell imaging to achieve single roll microtubes secured with a robust anchor to No. 1.5 coverslips.

Deposition and fabrication of SiN_x-based microtubes can be condensed to three crucial steps (Figure 4a–d): deposition of sacrificial layer and strained SiN_x bilayer, patterning and dry etch, and sacrificial layer etching, which releases built in strain and causes rolling from all unanchored sides. Strain, and thus diameter, in SiN_x microtubes is influenced by PECVD deposition parameters and postfabrication thermal processing.[42] Specifically, the sacrificial layer used here was either a (111) silicon substrate or germanium on a SiO_2 substrate. When fabricating biologically compatible rolled-up interfaces, it is intuitive that additional care must be taken to remove residual contamination before beginning a culture. Initially, Si (111) substrates were utilized as sacrificial layers due to a low vertical etch rate and low film porosity, achieving the most uniform arrays on silicon. Under SEM inspection (Figure 1c), sparse residue was identified on the substrate between microtubes. As an improvement over KOH etching, a germanium sacrificial layer was employed and successively etched in H_2O_2, which simultaneously cleaned the sample. In both cases the sacrificial layer is sonicated in acetone to remove any organic contamination and then subjected to a native oxide etch. If germanium is to be used, e-beam evaporated Ge is deposited at a rate of 1 nm/sec under 1–2 μTorr to a thickness of 20–80 nm. The strained bilayer consists of a 15–20 nm low frequency PECVD SiN_x (under compressive strain) capped by a 15–20 nm high frequency SiN_x (tensile). The mesa is patterned with AZ5214E and CF_4 is used to dry etch through the bilayer and into sacrificial layer. The photoresist is removed and the sacrificial layer is etched with 30% H_2O_2 at 80 °C for Ge and 45% KOH at 80C for Si.[42] Finally, the layers are immersed in methanol for 5 min and dried on hot plate at 80 °C. To achieve binocular shaped microtubes (Figure 1c) instead of single rolled microtubes, the initial mesa width must be equal to or larger than twice the final circumference. Per fabrication process #1 (Figure 4c), the sacrificial layer is removed from everywhere on the sample except a small anchor (~500 nm) under the microtube, exposing the underlying substrate and resulting in an elevated microtube (~20 nm). In contrast, process #2 (Figure 4d) results in microtubes anchored to the substrate and rolled from one side, removing the effect of this gap.

Preculture Microtube Preparation. The microtube-contained substrate was stored in 70% ethyl alcohol for cleaning and sterilizing. Prior to poly-D-lysine (PDL) coating, the sterilized substrate was carefully flooded by preautoclaved milli-Q deionized water three times to rinse off the alcohol. Beginning at this point, every following procedure was performed in a sterile environment. The substrate was subsequently dried and treated with UV exposure for 15 min, followed by PDL coating. Poly-D-lysine in a final concentration of 0.1 mg/mL was used to coat the substrate surface and facilitate cell adhesion.

Cortical Neural Culturing. For the axon guidance study, E15.5 cortical neurons obtained from Swiss Webster mice were used. Briefly, the cells were dissociated by treating with trypsin (0.25%, 15 min, 37 °C), then triturated, diluted in plating medium (neurobasal medium with 5% FBS, Hyclone, B27 supplement, 2 mMglutamine, 37.5 mMNaCl, and 0.3% glucose), and plated onto the substrates in a 35 mm Petri dish. Cells were seeded at either low density (5000 cells/cm^2) or high density (50 000 cells/cm^2) as indicated in the Results section. After 1 h, the sample was flooded with serum-free medium (plating medium without FBS) and cultured for 5–7 days, or as indicated elsewhere.

Immunostaining and Fluorescent Imaging. The culture sample for fluorescent imaging was fixed in 4% paraformaldehyde/Krebs/sucrose at pH 7.4, blocked with 10% BSA/PBS, permeabilized in 0.2% Trition X-100/PBS, and labeled with antibodies to tyrosinated tubulin at 1:1000 (YL1/2 clone, Chemicon[64]). Secondary antibodies coupled to Alexa 568 (Invitrogen) were used at 1:500. The immunostained cell cultures were imaged with a Fluoview500 AX70 upright (Olympus, USA) microscope through a 40× water-immersion lens of numerical aperture 0.8.

Sample Preparation and SEM Imaging. Prior to SEM imaging, the cell culture was fixed in mixed primary fixative of 2% paraformaldehyde/Krebs/sucrose and 2.5% glutaraldehyde in phosphate buffer at pH 7.4 for 30 min, then rinsed three times with phosphate buffered saline (PBS) solution. The cell culture was then treated with a postfixative of 1% osmium tetraoxide in phosphate buffer at pH 7.4 for 1 h, and then rinsed thoroughly with PBS solution. The fixed sample was dehydrated through an ethanol series with 10%–90%, and three times 100%, over 30 min. The dehydrated sample was then dried in a critical point dryer, and sputter-coated with ~2 nm gold–palladium. SEM images were taken with a LEO Gemini 1530 at 45° tilting.

Live Cell Imaging. The neural culture after 2–5 DIV was imaged using a BioStation integrated microscope (Nikon, Inc.) through a 20× lens. A phase contrast image was captured every 15 min for 18–48 h. Details of equipment setup was previously described.[6]

Conflict of Interest: The authors declare no competing financial interest.

Acknowledgment. Financial support for this project was provided in part by the Andrew T. Yang Research Award (P.F. and X.L.), NSF ECCS No. 1309375 (W.H. and X.L.), NSF STC CBET 0939511 Emergent Behavior of Integrated Cellular Systems (M.U.G.), IGERT 0903622 NeuroEngineering (O.V.C.), and NIH Grant NS080928 (E.W.D.). Technical discussions or assistance from R. Blick, K. J. Hsia, T. Saif, R. Gillette, M. Wang, and S. Robinson are gratefully acknowledged. We also thank T. M. Gomez for insights and technical support with fluorescent microscopy.

Supporting Information Available: Additional information for C−V analysis, FEM simulation, and growth statistics. This material is available free of charge *via* the Internet at http://pubs.acs.org.

REFERENCES AND NOTES

1. Pearce, T. M.; Williams, J. C. Microtechnology: Meet Neurobiology. *Lab Chip* **2007**, *7*, 30–40.
2. Taylor, D. M.; Tillery, S. I.; Schwartz, A. B. Direct Cortical Control of 3D Neuroprosthetic Devices. *Science* **2002**, *296*, 1829–32.
3. Berger, T. W.; Glanzman, D. *Toward Replacement Parts for the Brain: Implantable Biomimetic Electronics as Neural Prostheses*; MIT Press: Cambridge, MA, 2005; pp ix, 405.
4. Vitzthum, L.; Chen, X.; Kintner, D. B.; Huang, Y.; Chiu, S. Y.; Williams, J.; Sun, D. Study of Na+/H+ Exchange-Mediated Phi Regulations in Neuronal Soma and Neurites in Compartmentalized Microfluidic Devices. *Integr Biol.* **2010**, *2*, 58–64.
5. Hart, S. R.; Huang, Y.; Fothergill, T.; Lumbard, D. C.; Dent, E. W.; Williams, J. C. Adhesive Micro-line Periodicity Determines Guidance of Axonal Outgrowth. *Lab Chip* **2013**, *13*, 562–569.
6. Huang, Y.; Agrawal, B.; Clark, P. A.; Williams, J. C.; Kuo, J. S. Evaluation of Cancer Stem Cell Migration Using Compartmentalizing Microfluidic Devices and Live Cell Imaging. *J. Visualized Exp.* **2011**, *58*, e329710.3791/3297 .
7. Huang, Y.; Williams, J. C.; Johnson, S. M. Brain Slice on a Chip: Opportunities and Challenges of Applying Microfluidic Technology to Intact Tissues. *Lab Chip* **2012**, *12*, 2103–2117.
8. Berger, T. W.; Glanzman, D. *Toward Replacement Parts for the Brain: Implantable Biomimetic Electronics as Neural Prostheses*; MIT Press: Cambridge, MA, 2005.
9. Soe, A. K.; Nahavandi, S.; Khoshmanesh, K. Neuroscience Goes on a Chip. *Biosens. Bioelectron.* **2012**, *35*, 1–13.
10. Park, J. W.; Vahidi, B.; Taylor, A. M.; Rhee, S. W.; Jeon, N. L. Microfluidic Culture Platform for Neuroscience Research. *Nat. Protoc.* **2006**, *1*, 2128–2136.
11. Thompson, M.; Cheran, L.-E.; Sadeghi, S. *Sensor Technology in Neuroscience*; Royal Society of Chemistry: London, 2013.
12. Robinson, J. T.; Jorgolli, M.; Shalek, A. K.; Yoon, M.-H.; Gertner, R. S.; Park, H. Vertical Nanowire Electrode Arrays as a Scalable Platform for Intracellular Interfacing To Neuronal Circuits. *Nat. Nanotechnol.* **2012**, *7*, 180–184.
13. Vansteensel, M. J.; Hermes, D.; Aarnoutse, E. J.; Bleichner, M. G.; Schalk, G.; Van Rijen, P. C.; Leijten, F. S.; Ramsey, N. F. Brain−Computer Interfacing Based on Cognitive Control. *Ann. Neurol.* **2010**, *67*, 809–816.
14. Millet, L. J.; Gillette, M. U. New Perspectives on Neuronal Development *via* Microfluidic Environments. *Trends Neurosci.* **2012**, *35*, 752–61.
15. Moore, S. W.; Roca-Cusachs, P.; Sheetz, M. P. Stretchy Proteins on Stretchy Substrates: The Important Elements of Integrin-Mediated Rigidity Sensing. *Dev. Cell* **2010**, *19*, 194–206.
16. Discher, D. E.; Janmey, P.; Wang, Y.-L. Tissue Cells Feel and Respond to the Stiffness of Their Substrate. *Science* **2005**, *310*, 1139–1143.
17. Janmey, P. A.; Mcculloch, C. A. Cell Mechanics: Integrating Cell Responses to Mechanical Stimuli. *Annu. Rev. Biomed. Eng.* **2007**, *9*, 1–34.
18. Kerstein, P. C.; Jacques-Fricke, B. T.; Rengifo, J.; Mogen, B. J.; Williams, J. C.; Gottlieb, P. A.; Sachs, F.; Gomez, T. M. Mechanosensitive TRPC1 Channels Promote Calpain Proteolysis of Talin To Regulate Spinal Axon Outgrowth. *J. Neurosci.* **2013**, *33*, 273–285.
19. Bazaka, K.; Jacob, M. V. Implantable Devices: Issues and Challenges. *Electronics* **2012**, *2*, 1–34.
20. Williams, J. C.; Rennaker, R. L.; Kipke, D. R. Stability of Chronic Multichannel Neural Recordings: Implications for a Long-Term Neural Interface. *Neurocomputing* **1999**, *26*, 1069–1076.
21. Kapur, S. K.; Richner, T.; Brodnick, S.; Williams, J. C.; Poore, S. O. Development of an Optogenetic Sensory Peripheral Nerve Interface. *Plast. Reconstr. Surg.* **2014**, *133*, 10–99.
22. Schendel, A. A.; Thongpang, S.; Brodnick, S. K.; Richner, T. J.; Lindevig, B. D.; Krugner-Higby, L.; Williams, J. C. A Cranial Window Imaging Method for Monitoring Vascular Growth around Chronically Implanted Micro-ECoG Devices. *J. Neurosci. Methods* **2013**, *218*, 121–130.
23. Cogan, S. F. Neural Stimulation and Recording Electrodes. *Annu. Rev. Biomed. Eng.* **2008**, *10*, 275–309.
24. Boyden, E. S.; Zhang, F.; Bamberg, E.; Nagel, G.; Deisseroth, K. Millisecond-Timescale, Genetically Targeted Optical Control of Neural Activity. *Nat. Neurosci.* **2005**, *8*, 1263–1268.
25. Waser, R. *Nanoelectronics and Information Technology*; John Wiley & Sons: New York, 2012.
26. Rutten, W. L. Selective Electrical Interfaces with the Nervous System. *Annu. Rev. Biomed. Eng.* **2002**, *4*, 407–452.
27. Kotov, N. A.; Winter, J. O.; Clements, I. P.; Jan, E.; Timko, B. P.; Campidelli, S.; Pathak, S.; Mazzatenta, A.; Lieber, C. M.; Prato, M. Nanomaterials for Neural Interfaces. *Adv. Mater.* **2009**, *21*, 3970–4004.
28. Patolsky, F.; Timko, B. P.; Yu, G.; Fang, Y.; Greytak, A. B.; Zheng, G.; Lieber, C. M. Detection, Stimulation, and Inhibition of Neuronal Signals with High-Density Nanowire Transistor Arrays. *Science* **2006**, *313*, 1100–1104.
29. Fricke, R.; Zentis, P. D.; Rajappa, L. T.; Hofmann, B.; Banzet, M.; Offenhäusser, A.; Meffert, S. H. Axon Guidance of Rat Cortical Neurons by Microcontact Printed Gradients. *Biomaterials* **2011**, *32*, 2070–2076.
30. Martinez, D.; Py, C.; Denhoff, M.; Monette, R.; Comas, T.; Krantis, A.; Mealing, G. Polymer Peel-off Mask for High-Resolution Surface Derivatization, Neuron Placement and Guidance. *Biotechnol. Bioeng.* **2013**, *110*, 2236–2241.
31. Li, X. Strain Induced Self-Rolled-Up Ring Resonators: A Review of Geometrical and Resonant Properties. *Adv. Opt. Photonics* **2011**, *3*, 366–387.
32. Mei, Y.; Huang, G.; Solovev, A. A.; Urena, E. B.; Mönch, I.; Ding, F.; Reindl, T.; Fu, R. K.; Chu, P. K.; Schmidt, O. G. Versatile Approach for Integrative and Functionalized Tubes by Strain Engineering of Nanomembranes on Polymers. *Adv. Mater.* **2008**, *20*, 4085–4090.
33. Li, X. Strain Induced Semiconductor Nanotubes: From Formation Process to Device Applications. *J. Phys. D: Appl. Phys.* **2008**, *41*, 193001.
34. Mi, Z.; Bianucci, P. When Self-Organized in(Ga)Ss/GaAs Quantum Dot Heterostructures Roll up: Emerging Devices and Applications. *Curr. Opin. Solid State Mater. Sci.* **2012**, *16*, 52–58.
35. Schmidt, O. G.; Eberl, K. Nanotechnology: Thin Solid Films Roll up into Nanotubes. *Nature* **2001**, *410*, 168–168.
36. Prinz, V. Y.; Seleznev, V. A.; Gutakovsky, A. K.; Chehovskiy, A. V.; Preobrazhenskii, V. V.; Putyato, M. A.; Gavrilova, T. A. Free-Standing and Overgrown InGaAs/GaAs Nanotubes, Nanohelices and Their Arrays. *Phys. E* **2000**, *6*, 828–831.
37. Cavallo, F.; Grierson, D. S.; Turner, K. T.; Lagally, M. G. Soft Si: Effective Stiffness of Supported Crystalline Nanomembranes. *ACS Nano* **2011**, *5*, 5400–5407.
38. Cavallo, F.; Lagally, M. G. Semiconductors Turn Soft: Inorganic Nanomembranes. *Soft Matter* **2010**, *6*, 439–455.
39. Schulze, S.; Huang, G.; Krause, M.; Aubyn, D.; Quiñones, V. a. B.; Schmidt, C. K.; Mei, Y.; Schmidt, O. G. Morphological Differentiation of Neurons on Microtopographic Substrates Fabricated by Rolled-Up Nanotechnology. *Adv. Eng. Mater.* **2010**, *12*, B558–B564.

40. Yu, M.; Huang, Y.; Ballweg, J.; Shin, H.; Huang, M.; Savage, D. E.; Lagally, M. G.; Dent, E. W.; Blick, R. H.; Williams, J. C. Semiconductor Nanomembrane Tubes: Three-Dimensional Confinement for Controlled Neurite Outgrowth. *ACS Nano* **2011**, *5*, 2447–2457.
41. Bausch, C. S.; Koitmäe, A.; Stava, E.; Price, a.; Resto, P. J.; Huang, Y.; Sonnenberg, D.; Stark, Y.; Heyn, C.; Williams, J. C. Guided Neuronal Growth on Arrays of Biofunctionalized GaAs/InGaAs Semiconductor Microtubes. *Appl. Phys. Lett.* **2013**, *103*, 173705.
42. Froeter, P.; Yu, X.; Huang, W.; Du, F.; Li, M.; Chun, I.; Kim, S. H.; Hsia, K. J.; Rogers, J. A.; Li, X. 3d Hierarchical Architectures Based on Self-Rolled-Up Silicon Nitride Membranes. *Nanotechnology* **2013**, *24*, 475301.
43. Huang, W.; Yu, X.; Froeter, P.; Xu, R.; Ferreira, P.; Li, X. On-Chip Inductors with Self-Rolled-Up SiN_x Nanomembrane Tubes: A Novel Design Platform for Extreme Miniaturization. *Nano Lett.* **2012**, *12*, 6283–88.
44. Li Jeon, N.; Baskaran, H.; Dertinger, S. K. W.; Whitesides, G. M.; Van De Water, L.; Toner, M. Neutrophil Chemotaxis in Linear and Complex Gradients of Interleukin-8 Formed in a Microfabricated Device. *Nat. Biotechnol.* **2002**, *20*, 826–830.
45. Taylor, A. M.; Blurton-Jones, M.; Rhee, S. W.; Cribbs, D. H.; Cotman, C. W.; Jeon, N. L. A Microfluidic Culture Platform for CNS Axonal Injury, Regeneration and Transport. *Nat. Meth.* **2005**, *2*, 599–605.
46. Rall, W., Core Conductor Theory and Cable Properties of Neurons. in *Comprehensive Physiology*; John Wiley & Sons, Inc.: New York, 2011.
47. Wang, L.; Riss, M.; Buitrago, J. O.; Claverol-Tinturé, E. Biophysics of Microchannel-Enabled Neuron−Electrode Interfaces. *J. Neural Eng.* **2012**, *9*, 026010.
48. Grill, W. M.; Norman, S. E.; Bellamkonda, R. V. Implanted Neural Interfaces: Biochallenges and Engineered Solutions. *Annu. Rev. Biomed. Eng.* **2009**, *11*, 1–24.
49. Fields, R. D.; Le Beau, J. M.; Longo, F. M.; Ellisman, M. H. Nerve Regeneration through Artificial Tubular Implants. *Prog. Neurobiol.* **1989**, *33*, 87–134.
50. Dent, E. W.; Gertler, F. B. Cytoskeletal Dynamics and Transport in Growth Cone Motility and Axon Guidance. *Neuron* **2003**, *40*, 209–27.
51. Hur, E.-M.; Yang, I. H.; Kim, D.-H.; Byun, J.; Saijilafu; Xu, W.-L.; Nicovich, P. R.; Cheong, R.; Levchenko, A.; Thakor, N.; Zhou, F.-Q. Engineering Neuronal Growth Cones To Promote Axon Regeneration Over Inhibitory Molecules. *Proc. Natl. Acad. Sci. U.S.A.* **2011**, *108*, 5057–5062.
52. Shi, P.; Nedelec, S.; Wichterle, H.; Kam, L. C. Combined Microfluidics/Protein Patterning Platform for Pharmacological Interrogation of Axon Pathfinding. *Lab Chip* **2010**, *10*, 1005–1010.
53. Craig, E. M.; Van Goor, D.; Forscher, P.; Mogilner, A. Membrane Tension, Myosin Force, and Actin Turnover Maintain Actin Treadmill in the Nerve Growth Cone. *Biophys. J.* **2012**, *102*, 1503–13.
54. Huang, H.; Winchester, K.; Suvorova, A.; Lawn, B.; Liu, Y.; Hu, X.; Dell, J.; Faraone, L. Effect of Deposition Conditions on Mechanical Properties of Low-Temperature PECVD Silicon Nitride Films. *Mater. Sci. Eng.: A* **2006**, *435*, 453–459.
55. Colombi, P.; Bergese, P.; Bontempi, E.; Borgese, L.; Federici, S.; Keller, S. S.; Boisen, A.; Depero, L. E. Sensitive Determination of the Young's Modulus of Thin Films by Polymeric Microcantilevers. *Meas. Sci. Technol.* **2013**, *24*, 125603.
56. Saha, K.; Keung, A. J.; Irwin, E. F.; Li, Y.; Little, L.; Schaffer, D. V.; Healy, K. E. Substrate Modulus Directs Neural Stem Cell Behavior. *Biophys. J.* **2008**, *95*, 4426–4438.
57. Chen, S.; Liu, L.; Zhou, J.; Jiang, S. Controlling Antibody Orientation on Charged Self-Assembled Monolayers. *Langmuir* **2003**, *19*, 2859–2864.
58. Cai, K.; Frant, M.; Bossert, J.; Hildebrand, G.; Liefeith, K.; Jandt, K. D. Surface Functionalized Titanium Thin Films: Zeta-Potential, Protein Adsorption and Cell Proliferation. *Colloids Surf., B* **2006**, *50*, 1–8.
59. Kirby, B. J.; Wheeler, A. R.; Zare, R. N.; Fruetel, J. A.; Shepodd, T. J. Programmable Modification of Cell Adhesion and Zeta Potential in Silica Microchips. *Lab Chip* **2003**, *3*, 5–10.
60. Bondar, O. V.; Saifullina, D. V.; Shakhmaeva, Ii; Mavlyutova, Ii; Abdullin, T. I. Monitoring of the Zeta Potential of Human Cells upon Reduction in Their Viability and Interaction with Polymers. *Acta Nat.* **2012**, *4*, 78–81.
61. Nishi, Y.; Doering, R. *Handbook of Semiconductor Manufacturing Technology*; CRC Press: Boca Raton, FL, 2000.
62. Loux, N. T.; Savage, N. An Assessment of the Fate of Metal Oxide Nanomaterials in Porous Media. *Water, Air, Soil Pollut.* **2008**, *194*, 227–241.
63. Helland, S. *Electrical Characterization of Amorphous Silicon Nitride Passivation Layers for Crystalline Silicon Solar Cells*. M.S. Thesis, Norwegian University of Science and Technology, Trondheim, Norway, 2011
64. Dent, E. W.; Kalil, K. Axon Branching Requires Interactions between Dynamic Microtubules and Actin Filaments. *J. Neurosci.* **2001**, *21*, 9757–9769.
65. Chun, I. S.; Challa, A.; Derickson, B.; Hsia, K. J.; Li, X. Geometry Effect on the Strain-Induced Self-Rolling of Semiconductor Membranes. *Nano Lett.* **2010**, *10*, 3927–3932.
66. Huang, W.; Koric, S.; Yu, X.; Hsia, K. J.; Li, X. Precision Structural Engineering of Self-Rolled-up 3D Nanomembranes Guided by Transient Quasi-Static FEM Modeling. *Nano Lett.* **2014**, DOI: 10.1021/nl5026369.